Technical Report
RAL-TR-2001-042

CLRC

CFD Simulations of Convective Heat Transfer in the Atlas SCT End-Cap

R F Fowler and C Greenough

29th November 2001

COUNCIL FOR THE CENTRAL LABORATORY OF THE RESEARCH COUNCILS

Enquiries about copyright, reproduction and requests for additional copies of this report should be addressed to:

The Central Laboratory of the Research Councils
Library and Information Services
Rutherford Appleton Laboratory
Chilton
Didcot
Oxfordshire
OX11 0QX
Tel: 01235 445384 Fax: 01235 446403
E-mail library@rl.ac.uk

ISSN 1358-6254

CFD Simulations of convective heat transfer in the Atlas SCT End-Cap

R.F.Fowler and C.Greenough,
Rutherford Appleton Laboratory,
Chilton, Didcot OX11 0QX, UK
Email: r.f.fowler@rl.ac.uk

05 Oct 2001

Abstract

The convective heat transfer process within the End-cap detector of the Atlas SCT has been modelled using the CFD package CFX. Predictions of the levels of heat flux across sensitive parts of the detector are given for 2 and 3D approximations of the actual system.

Keywords: Computational fluid dynamics, Heat transfer, CFX

Contents

1 Introduction **1**

2 Geometry of the Model **1**

3 Simulations details **2**

3.1 Boundary conditions 2

3.2 Physical models 3

3.3 2D simulations 4

3.4 3D simulations 4

3.5 3D approach to equilibrium 7

4 Results **8**

4.1 2D Results 8

4.2 3D results 11

4.2.1 Temperature profiles and flow patterns 11

4.2.2 Heat flux results 11

5 Summary **26**

1 Introduction

The Atlas detector is being built to study proton-proton collisions in the new Large Hadron Collider (LHC) at CERN. The complete system will fully enclose the point at which particle collisions occur and consists of a number of different detectors to analyse the products of each event. A description of the main features of the system can be found on the Atlas web page: `http://atlas.web.cern.ch/Atlas`.

Each set of detectors within the Atlas assembly will have an electronic system to record the observed events. The power dissipated must be removed by cooling systems, to keep both the electronics and sensitive detector elements within required operating temperatures. In the case of the SemiConductor Tracker (SCT) End-cap, cooling is provided by a system of pipes through which circulates a refrigerant fluid. While there is sufficient cooling to remove the heat generated within the electronics, it is also important to ensure that no sensitive components will be above their maximum rated temperature during operation of the system. Computational and experimental modelling is being used to predict the steady state heat distribution in the system. This report focuses on the contribution of heat convection to the temperature distribution, using the CFD and thermal modelling package CFX [1].

The simulation results presented here are based on a simplified model of both the geometry of the enclosure and the thermal boundary conditions. Hence they can only provide a qualitative guide to the areas in which greatest heat transfer through convection will occur.

2 Geometry of the Model

The detector modules of the SCT End-cap are placed on annular surfaces (discs) with an inner radius of $R_i = 0.274m$ and an outer radius of $R_o = 0.560m$. Several of these discs are used, with increasing spacing, as illustrated in Figure 1. The detector modules, cooling pipes and power tapes on the surface of each annulus are quite complex and these are not shown in the diagram. The discs are held in position at their outer radius (R_o) by a cylindrical enclosure which contains apertures through which the various services pass. Outside this support cylinder is a solid cylindrical active thermal enclosure. There is an additional insulating cylindrical thermal enclosure at the inner radius (R_i). For this analysis these cylindrical boundaries are modelled as simple solid insulating walls. The space between the inner and outer cylinders is filled with dry nitrogen gas. A weak flow of nitrogen is maintained through the system, but this is very slow and is not thought to contribute significantly to cooling.

The spacing between detector planes varies from approximately 0.043m to of the order of 0.3m. Simulations have been concentrated on the small spacing cases as these are more likely to have excessive heat transfer problems. To investigate the dependence of the results on separation, simulations have been made with a gaps of 0.043m and 0.086m. The components mounted on the surface of the planes make the actual separation to use rather ill-defined so it is important to investigate the sensitivity of the results to this parameter.

The geometry of the problem is symmetric about the vertical plane ($x = 0$, where y is upwards and z is along the cylinder axis, as shown in the figure). To save on computation time, the 3D flow simulations will be taken as symmetric about this plane, and hence the geometry used is only one half of the full annular region between two discs.

All the simulation results assume smooth featureless side walls. This simplification means the results will be of a more qualitative nature, but given the size and complexity of the volume, and other uncertainties in the data for heat production, it would be extremely expensive to

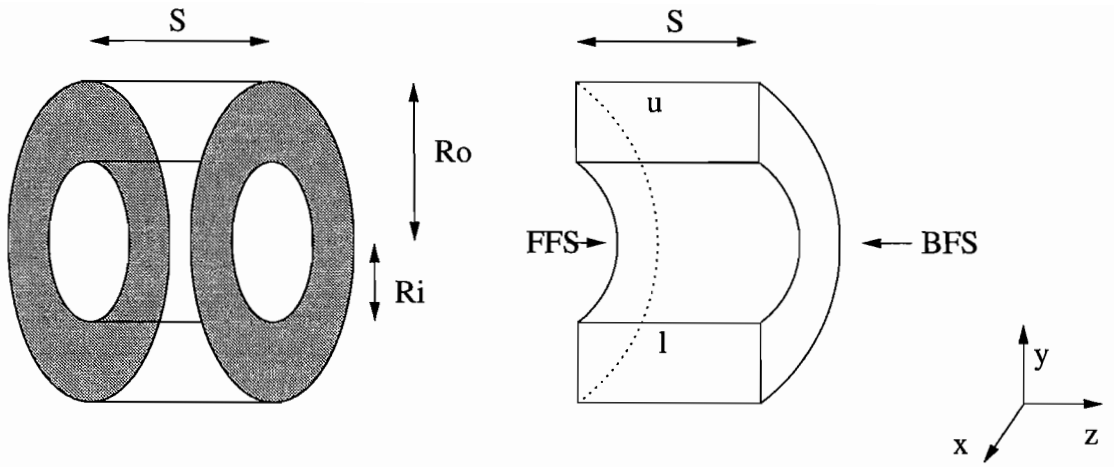

Figure 1: Left: schematic view of the arrangement of detectors in the SCT End-cap. Each shaded area represents an annular plane (or disc) on which detectors and their associated electronics and cooling systems are built. Walls exist at the inner radius R_i and the outer radius R_o. Different detector arrangements exist on the forward and backward facing sides of each plane. Right: View of the actual volume used in the simulations. The upper (u) and lower (l) faces have symmetry boundary conditions while the front of the disc (FFS, forward facing sidewall) and rear (BFS) have fixed temperature conditions.

do significantly better. Even with the simple model used here, the computational costs of 3D simulations is high. To get a better understanding of the sensitivity of the results to the mesh resolution we have performed some simulations on a 2D section through the top of the annulus, on the $x = 0$ plane.

3 Simulations details

The CFX software provides the preprocessor CFX-MESHBUILD to create the problem geometry and define the solution mesh. The output of MESHBUILD can then be read by the SOLVER module in conjunction with a run file that describes the physical models and boundary conditions to be used. Complex boundary conditions, such as wall temperature profiles, can be defined in a Fortran subroutine which is linked with the solver code. Postprocessing is provided via the CFX-VIEW module.

CFX also market an additional software module to deal with heat transfer through radiation effects. However this module was not installed on the system available for use in this project. Radiation effects become more important the higher the temperature difference, ΔT, in the system is. It is thought that radiation effects will be relatively weak in this case, as ΔT is not very large, $\approx$ 25K.

3.1 Boundary conditions

Only three types of boundary conditions have been used in these simulations:

- Fixed wall temperature. This boundary condition is used on the disc walls where electronic detectors generate heat and cooling pipes remove it. The temperature profile is derived from thermal simulations of the solid devices. The results have then been averaged to

give a simple temperature that is a function only of radius along the sidewall. Two such functions are defined, one for the front of the disc which holds inner and outer modules and one for the back of the disc which holds only middle modules. The use of fixed temperature is an approximation, since the convective heat transfer will alter surface temperatures.

- Zero heat flux walls. For the inner and outer walls very little heat flux is expected as the material is of low thermal conductivity and they are designed to be insulating. For sections of the discs inbetween the modules there is a complex mix pipes and power tapes. For simplicity these regions are also approximated as being of zero heat flux.
- Symmetry boundary conditions. These are used on the upper and lower faces of the half annulus ($x = 0$ plane) so as to reduce the problem size in 3D simulations. In unsteady flow it is possible that these boundary conditions will suppress some real non-symmetric oscillations. It is thought that this will be a very small effect in comparison with other approximations that have already been made, such as for the geometry and temperature profiles.

The default side wall temperature profiles used are shown in Figure 2. The front of the disc (labelled as forward facing sidewall, FFS) has two rings of modules and hence two high temperature peaks as a function of radius. The rear of each disc (labelled backward facing sidewall, BFS) has only one ring of modules and so has just one such peak. In one simulation the height of these three peaks will be reduced by 10K to investigate what effect such reduced operating temperature will have on heat flux due to convection.

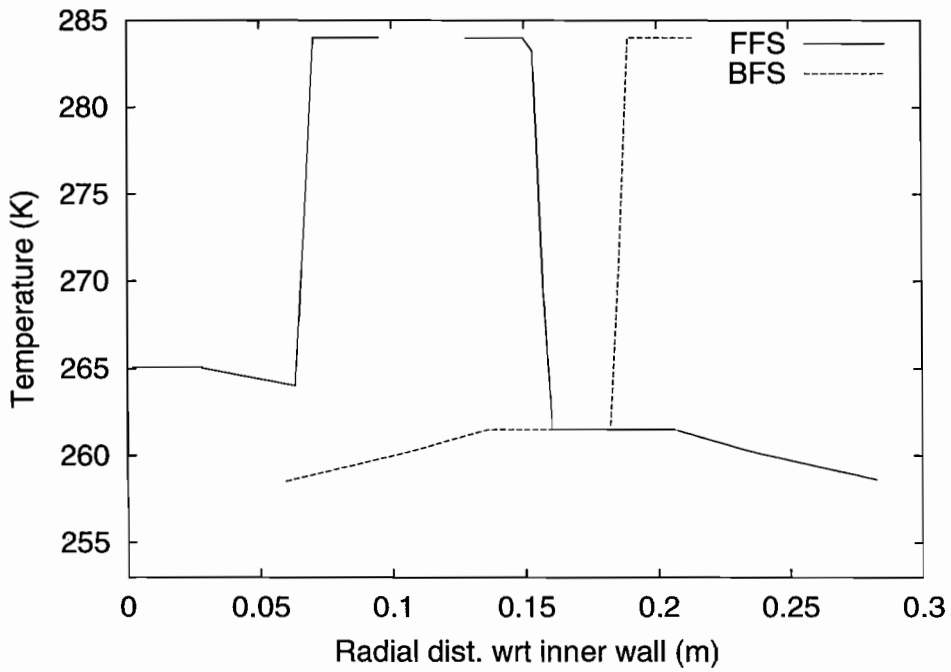

Figure 2: Radial temperature profiles used in the simulations. Points where the graphs have no value are taken as having zero heat flux. The two separate sidewalls (FFS and BFS) are shown on this one graph. For the simulation m07, the heights of the three peaks were all reduced by 10K.

3.2 Physical models

The CFX physical models used during for these simulations are:

- Fluid is dry nitrogen gas at atmospheric pressure.
- Heat transfer modelling is included.
- Buoyant flow is modelled. This is a simpler model than fully compressible flow but is adequate for this case.
- Transient simulations are used in all cases. Static simulations failed to converge. The Rayleigh Numbers of these problems indicates that unsteady flow is likely and there is clear evidence of this in the 3D results.
- Turbulent flow is modelled using the Wilcox low Reynolds Number turbulence model. This is appropriate for Reynolds numbers below about 30000. In most cases, though some turbulence is seen in the initial transient phase, the final state has very little turbulence.

Since there is no imposed flow in these simulations it is not possible to define a Reynolds Number for the flow in advance. Instead the Rayleigh Number, Ra [2], is sometimes used to characterise such convective flows with heat transfer. The Rayleigh number can be computed from:

$$R_a = \frac{g\,\beta\,\Delta T\,D^3}{\nu\,\alpha} \tag{1}$$

where g is the gravitational force, ΔT is the difference in temperature across the domain, D is a characteristic length of the problem, ρ is the gas density, ν is the kinematic viscosity, α is the thermal diffusivity and β in the volumetric expansion coefficient. Clearly this number is very sensitive to the characteristic length of the problem, D. If this is taken as the separation between the two sidewalls, this gives $R_a \approx 2 \times 10^6$ for $d = 0.086$m and $R_a \approx 3 \times 10^5$ for $d = 0.043$m.

For R_a above about 3×10^5 unsteady convective flows occur and turbulent flow is expected for $R_a \approx 10^6$ [2]. Thus our simulations are expected to show unsteady behaviour with perhaps small levels of turbulence. Using the actual observed flow velocity from the solution gives a Reynolds number of the order of 1000 for these simulations. This is consistent with turbulence being very weak in these systems.

3.3 2D simulations

Since the computational cost of 3D simulations is high, some 2D calculations were made along the section at the top of the annular region, on the $x = 0$ plane. A typical computational mesh is shown in Figure 3.

As noted above, a solution could only be obtained via a transient calculation. Monitoring the temperature and velocity components at one point in the lower half of the simulation domain gives results such as those shown in Figures 4 and 5. For this particular point it seems that a fairly steady temperature and velocity is reached after about 60 seconds of real time. It is likely that small oscillations are still present in other parts of the system which have not been monitored.

3.4 3D simulations

Figure 6 shows a view of the mesh used for the 3D simulations. This contains $17 \times 30 \times 60$ nodes, giving a total of 30600. Note that some weighting has been used to enhance the mesh resolution near the important sidewalls where the driving thermal interactions will occur. The radial mesh distribution has been left as uniform since reasonable resolution of the sidewall

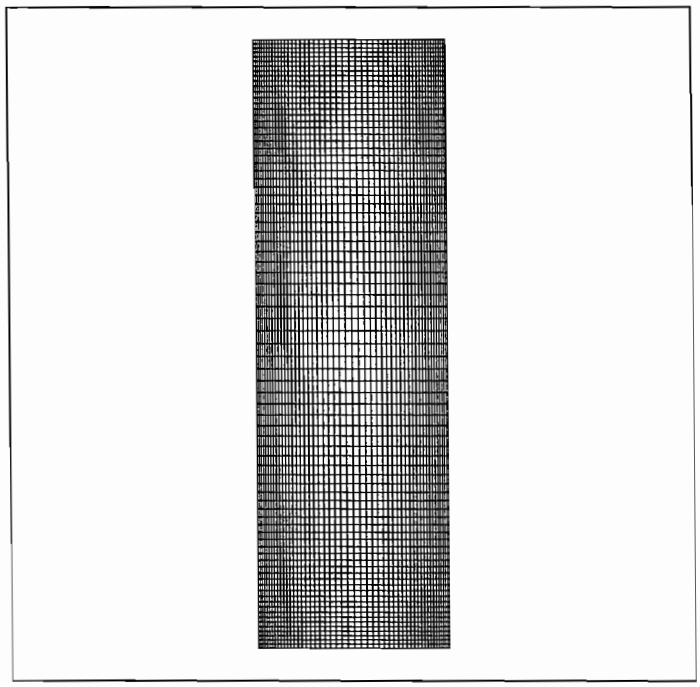

Figure 3: A typical mesh used for the 2D simulations. This has $50 \times 80 \times 1$ elements with weighting to give better resolution near the walls. There is zero heat flux on the top and bottom walls, while the sidewalls have the temperature profiles shown in Figure 2.

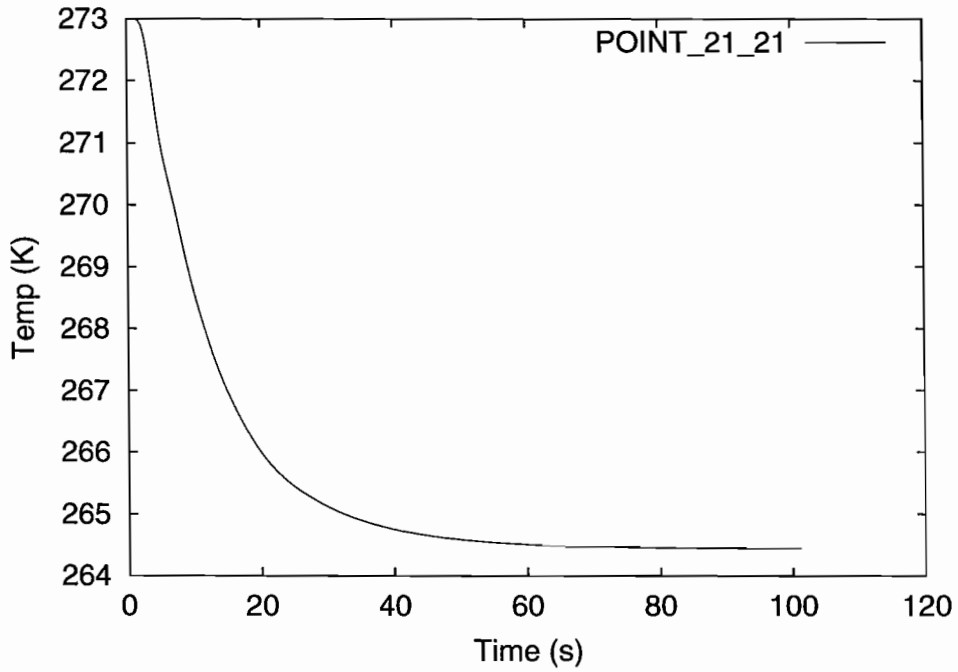

Figure 4: Time dependence of temperature during a 2D simulation started with constant temperature. The results refer to a central point away from the main flow regions.

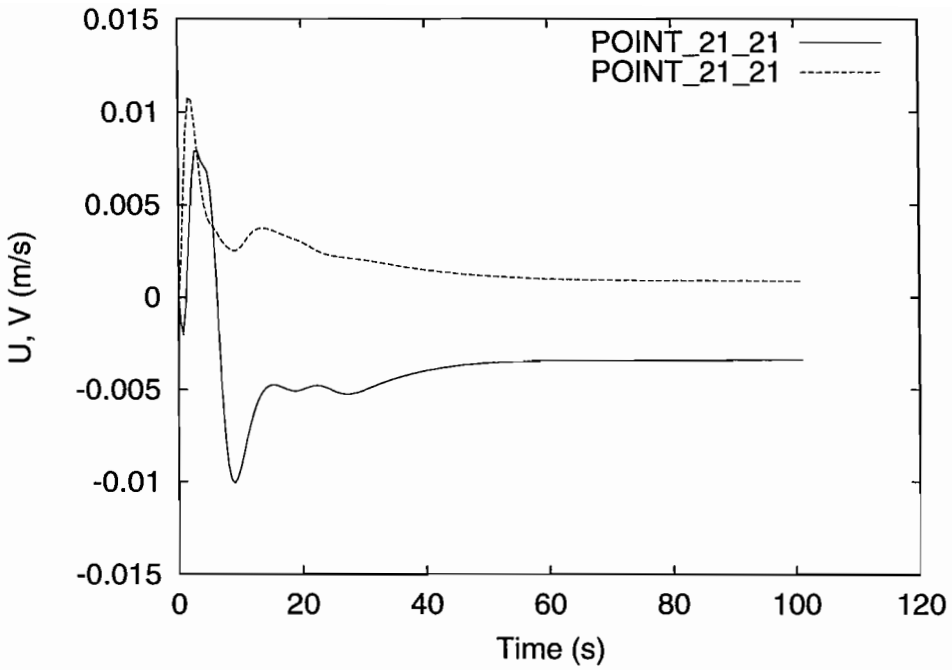

Figure 5: Time dependence of U and V velocity components for the same point as in Figure 4.

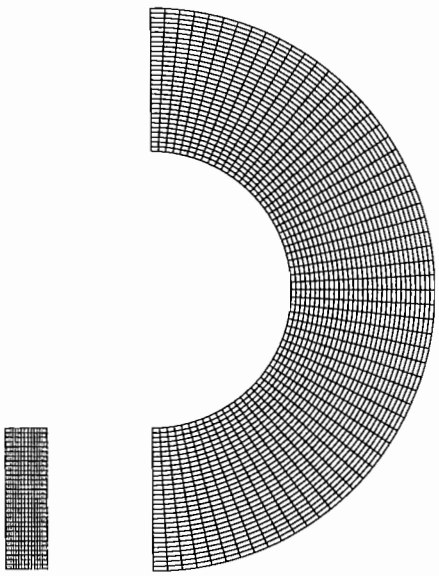

Figure 6: Views of the 3D mesh. The side view (right) shows the uniform resolution in angular and radial directions. Resolution has been increased toward the side walls in the z direction, as shown in the end view (left).

temperature profile is necessary and the inner and outer walls make no contribution to the heat transfer process.

3D simulations have been made for three different cases which are listed in Table 1. The run labels m02, m05 and m07 are used to distinguish these cases. The two different wall separations are used to investigate the effect of changing this parameter (m02, $0.086m$ vs m05, $0.043m$). In the final simulation (m07) the same sidewall temperature profiles have been used, except that the three high temperature peaks have been reduced by $10K$. The same number of mesh elements and nodes have been used in all the simulations. This means that the mesh resolution in z is improved in the two simulations with reduced wall spacing.

Run name	Wall gap (m)	Peak Temp. (K)	CPU time (s)	Max Speed (m/s)
m02	0.086	+30	10780	0.179
m05	0.043	+30	13044	0.225
m07	0.043	+20	8907	0.149

Table 1: Parameters of the 3D simulation cases. "Max speed" is the largest value seen in the final solution. The peak temperature refers to the height of the peaks in Figure 2.

In all simulations the temperature of the system was monitored at a selection of fixed points. Because these points are defined in terms of the grid element labels (`I,J,K`) rather than in real coordinates, the points in run m02 are not directly comparable with those from runs m05 and m07. Simulations were run for 140 seconds of real time in all cases.

The maximum flow speed in the three cases is also listed in Table 1. Reducing the gap between the sidewalls is seen to increase the maximum value by about 25%. Reducing the heat peak temperature means a reduced driving force and the maximum speed in m07 is about 30% less than in m05.

3.5 3D approach to equilibrium

As was noted for the 2D results and the Rayleigh number calculations there is evidence that the flow is unsteady and has persistent oscillations in both temperature and velocity. Such oscillations are still seen in the all the 3D simulations. A typical plot of the temperature variation in the three cases is shown in Figure 7. Similar oscillations are also seen in some of the velocity components.

At the selected point, it can be seen that there are larger temperature oscillations in m05 and m07, the simulations with the smaller gap, than in m02. However, on other monitored points the situation is reversed, with larger oscillations seen in m02. This indicates that the flow pattern is altered by the narrower sidewall separation. At this particular point it is found that the reduced separation gives a temperature perhaps 1K higher (on average) going from m02 to m05. The reduction of 10K in the high temperature peaks (m07) reduces this central temperature by about 4K and also reduces the frequency of the oscillations. These observations only apply to this single point and should not be taken as indicative of the changes across the whole device. More details of the temperature distributions are given in the following section on the results.

In all the simulations it was found that the level of turbulent kinetic energy in the final state was quite low. Higher levels of turbulence occur during the approach to equilibrium.

It appears that simulation runs of about 100 seconds are required to let the systems reach a reasonably steady state. All three simulations were run for 140 seconds. Simulation CPU times for these runs on the Columbus Alpha based system at RAL were typically about 2.5 hours.

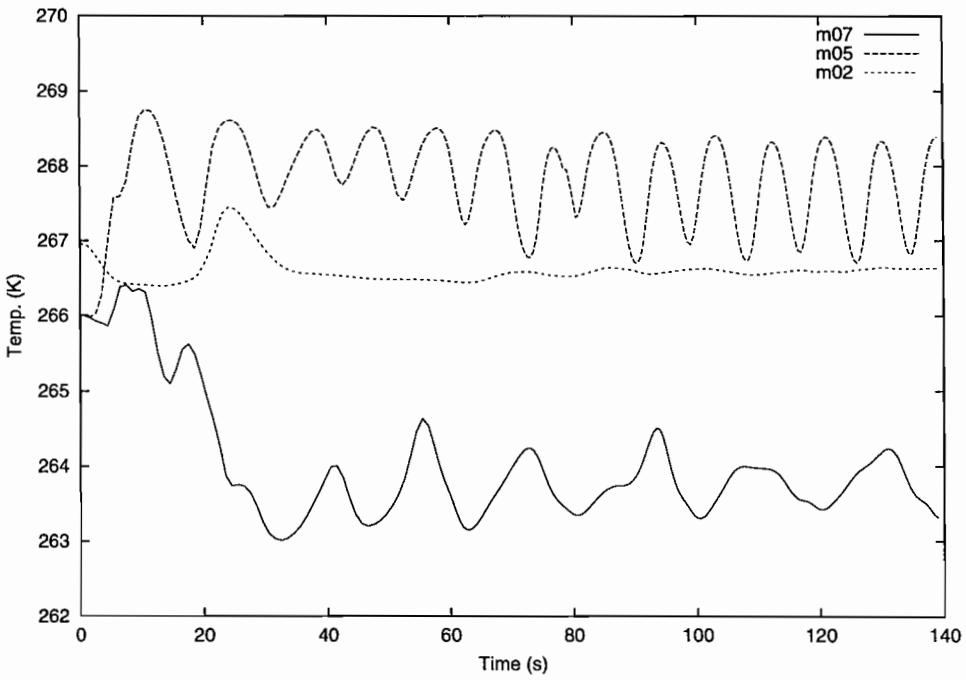

Figure 7: Temperature as a function of time during the simulations at the grid point (9,15,30), which is near the centre of the annulus, half way between top and bottom. Though the m02 temperature profile is fairly steady at this point, other points show at least as much temperature oscillation as seen here for m05 and m07. These results are typical of certain points within each simulation, though other points show much more steady temperatures.

4 Results

4.1 2D Results

The 2D simulations have been used to investigate mesh dependence of the results and to see the type of flow patterns which may be expected near the top of the enclosure. Figure 8 shows typical flow patterns for a simulation with a gap of 0.086m. Flow is seen to mostly be close to the sidewalls except where falling cool gas meets rising heated gas about half way up the FFS (left of figure). This results in a flow across to the BFS and a "figure of eight" pattern.

The temperature profile down the centre line ($x = 0.043$) half way between the two side walls is shown in Figure 9 for three different mesh resolutions, 13×25, 42×42 and 42×72. While the temperature profile does change with mesh density, the overall flow pattern is not altered. The coarse mesh profile is of the order of 1K lower in the upper part of the domain. The 3D mesh that was actually used has a resolution of 17×30 in these two dimensions, which is between the coarse and medium resolution used in 2D. Hence we may expect some error in the 3D results due to the coarseness of the mesh, but the general flow patterns should be correct.

The heat flux through the side walls is shown for two different mesh resolutions in Figures 10 and 11. Clearly some of the detail seen in the fine mesh calculation is lost with the coarse mesh. However, the coarse mesh results are reasonable, given the other uncertainties due to the geometrical and boundary condition approximations.

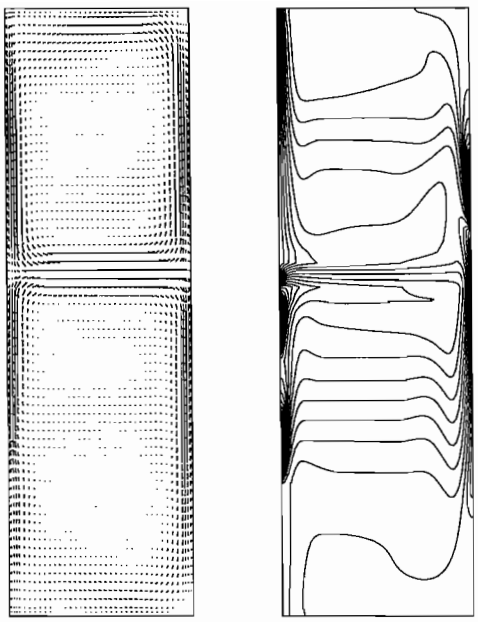

Figure 8: Left: vectors of velocity in a typical 2D simulation with 0.086m between the side walls. Right: Temperature contours for the same state.

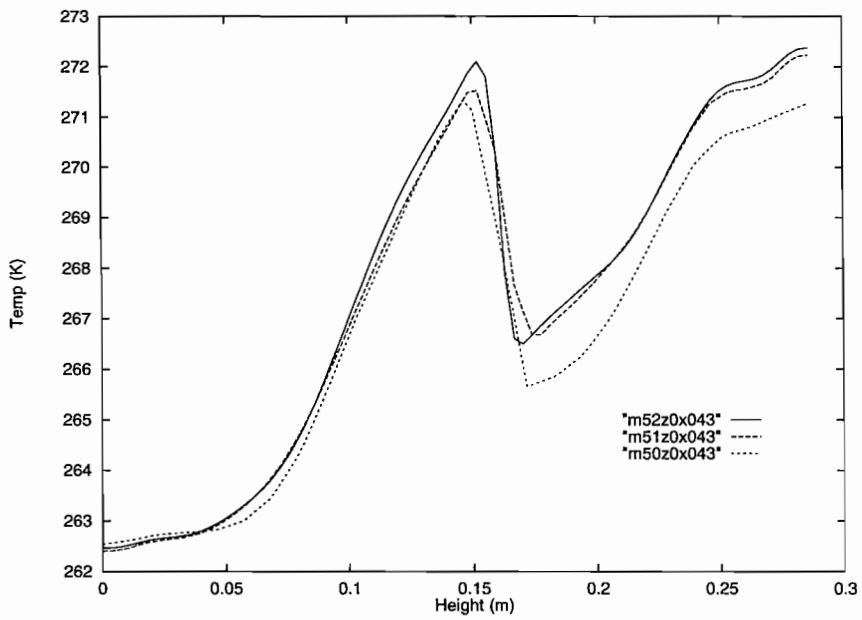

Figure 9: The 2D temperature profile along the centre line ($x = 0.043$m) half way between the two side walls. Results are shown from 3 calculations at increasing mesh resolution. M52 refers to the 42×72 node mesh, M51 to 42×42 and M50 to 13×25.

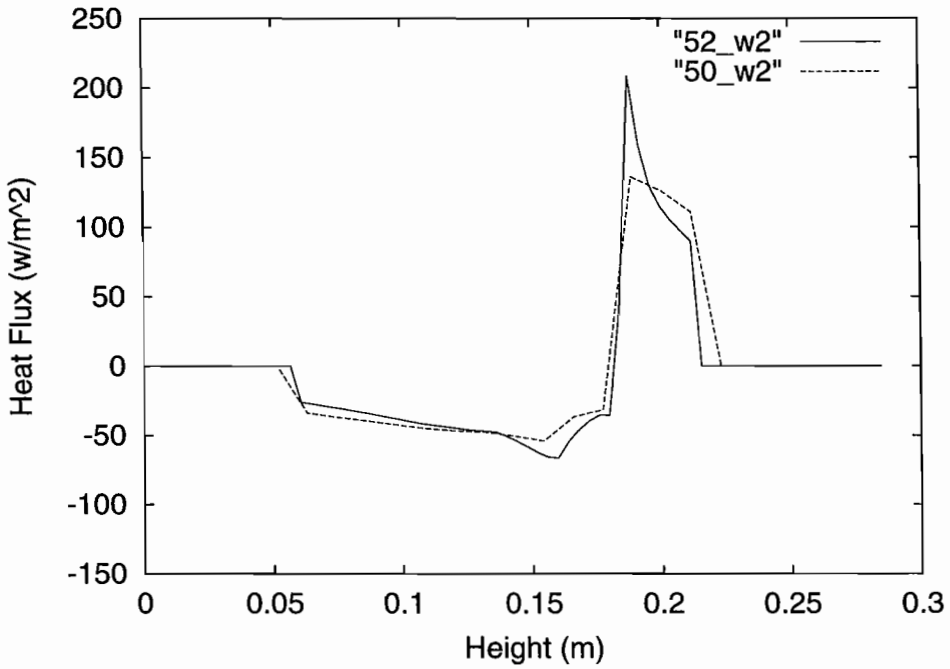

Figure 10: 2D heat flux through the FFS surface. The solid line is the result with a high mesh resolution and the dotted line with a coarse mesh. The height is measured from the inner wall (the lower wall in 2D).

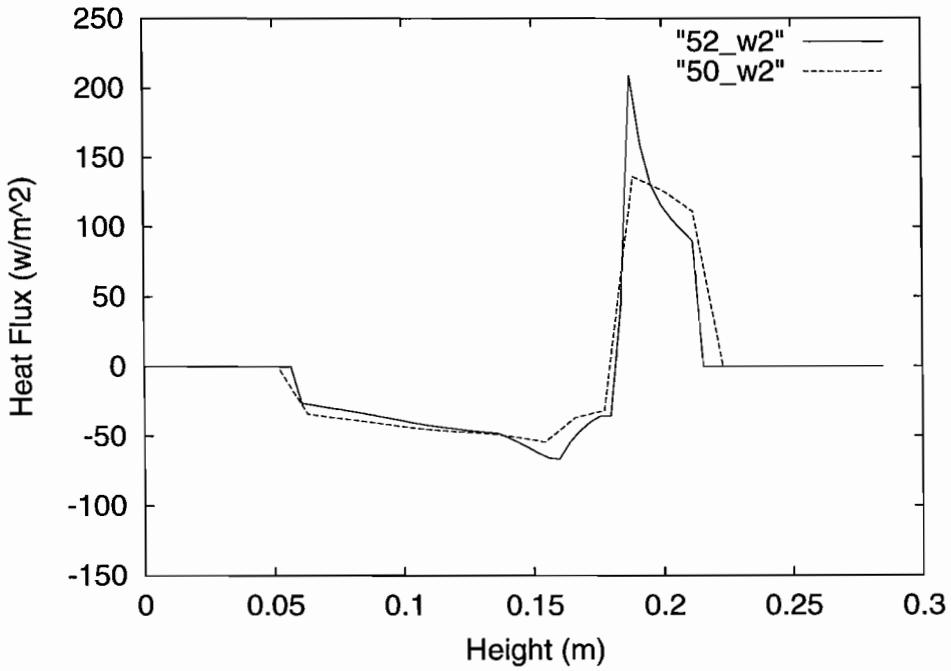

Figure 11: 2D heat flux through the BFS surface. The solid line is the result with a high mesh resolution and the dotted line with a coarse mesh.

4.2 3D results

4.2.1 Temperature profiles and flow patterns

Contour plots of the temperature profile on the cut plane midway between the two sidewalls are shown in Figures 21, 22 and 23. In each plot the colour scale runs between the minimum and maximum temperature in the system, so m02 and m05 can be directly compared. This is not the case for m07 as it has a more compressed scale.

There are some similar features between the temperature profiles, but they are certainly not identical. The actual temperature profile is thought to be less important than the heat flux that results from it.

Three vector plots of the flow pattern for case m02 are shown in Figure 20. These show that the convective flow in 3D is quite complex, and more difficult to understand than for the 2D case. The flow patterns do change slightly between runs, which contributes to the changes in heat flux reported in the following section.

4.2.2 Heat flux results

While the CFX postprocessor can easily provide contour plots of temperature on any cut plane, it appears more difficult to extract similar plots of the surface heat flux data. The data is listed in the output files from each simulation but there appears to be no option in CFX-View to read this section. Hence a separate program, Plotmtv, has been used to create colour contour plots of heat flux on the sidewalls. Unfortunately this program can only deal with rectangular domains. Hence sidewalls, which are actually "C" shaped like the cut plane in Figure 21, are mapped on to rectangular regions, such as Figure 24. The x-axis represents the distance from the inner wall while the y-axis is the angle (in degrees) measured from vertically downwards. Note that the contours are coloured in a non-uniform way with higher resolution in the areas of flow into the wall and lower resolution of the flow out of the wall.

Six separate plots are shown of the heat flux on the forward and backward facing sidewalls for each of the three cases: m02, m05 and m07. These are Figures 24 to 29. In this case the same colour scale is used across all the plots so they can be directly compared. Note that the parts of the surfaces with zero heat flux on them tend to have a speckled pattern as there is a contour level at zero and the data has some noise about this value.

The results show that there is a significant heat flux into the forward facing side at the very top of the annulus, as might be expected. It also shows a lot of heat flow into the band just above the high temperature areas in the lower half of the device.

A series of 1D plots have been made through the heat flux data on the two sidewalls to allow better comparison of the results. The two effects are the decrease in the spacing going from m02 to m05 and the reduction in the peak temperature from m05 to m07. Plots have been made at angles of 0 (vertical, downwards), 45, 90 (horizontal) and 180 degrees (vertical, upwards). In each graph the three separate results are plotted, all using the same scale.

In several cases, such as Figures 12 and 19, the narrowing of the gap between m02 and m05 seems to result in a larger peak value of the heat flow into the lower temperature regions. The reduction of the peak temperature in m07 generally cuts these peak values quite significantly.

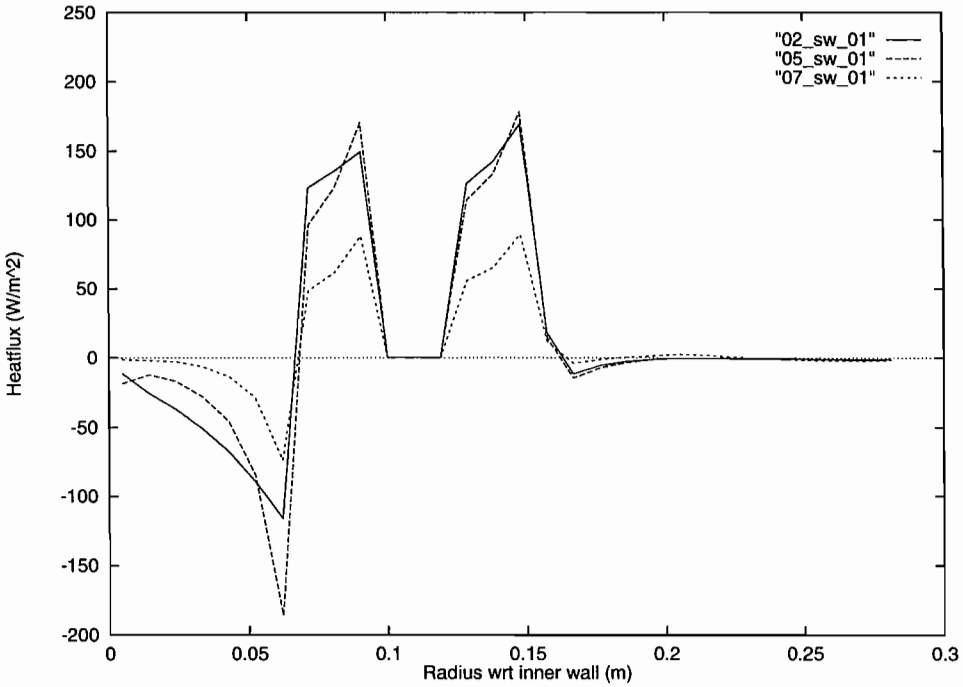

Figure 12: Heat flux on forward facing sidewall along radial direction 0 degrees, vertical downwards. "02_sw_01" refers to run m02, etc.

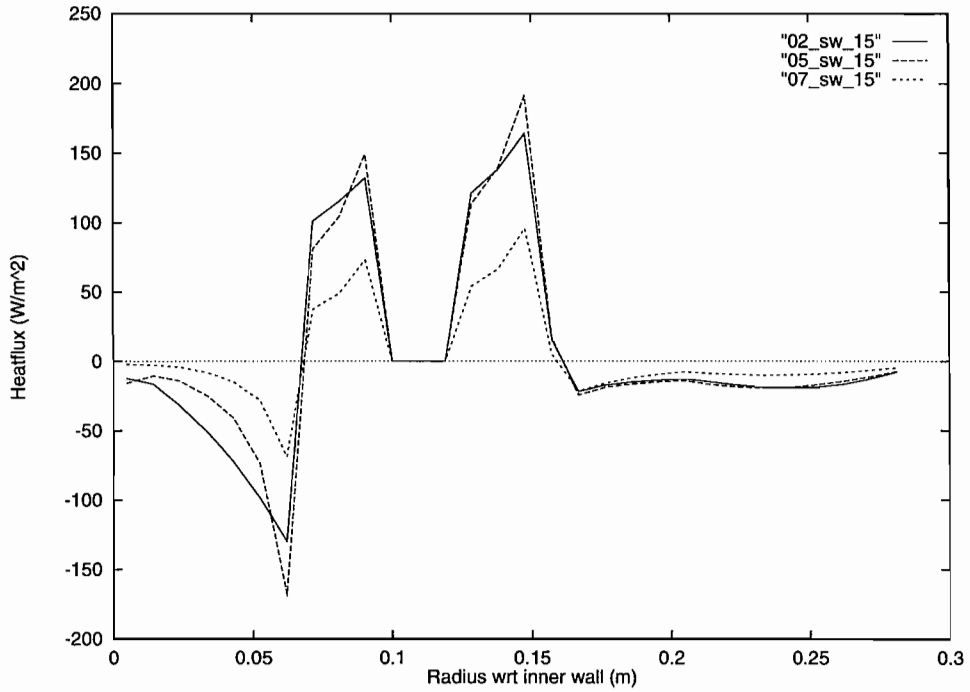

Figure 13: Heat flux on forward facing sidewall along radial direction 45 degrees.

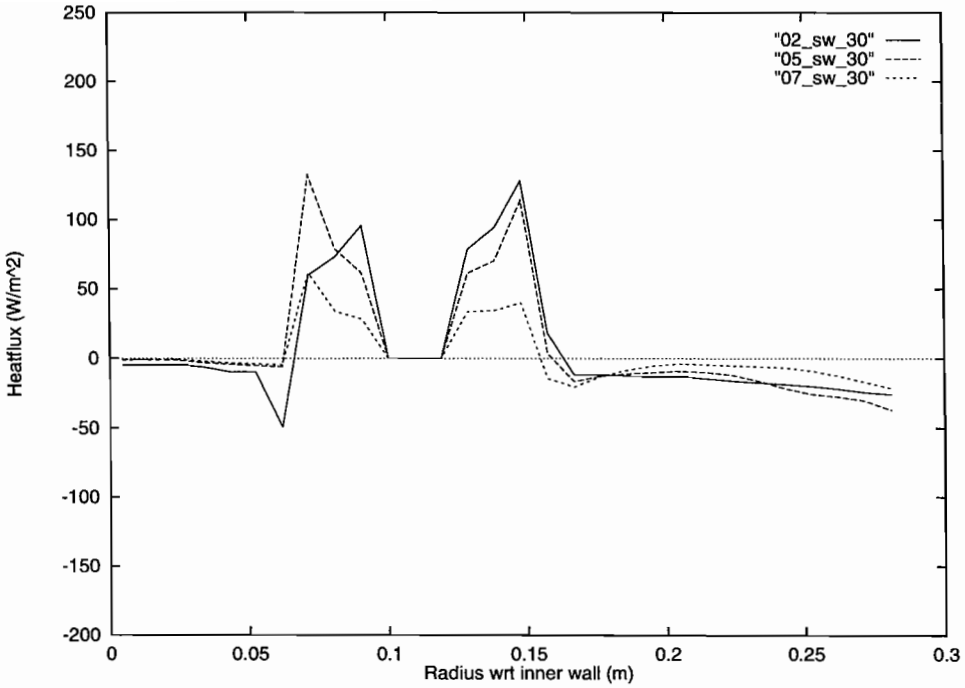

Figure 14: Heat flux on forward facing sidewall along radial direction 90 degrees, horizontal.

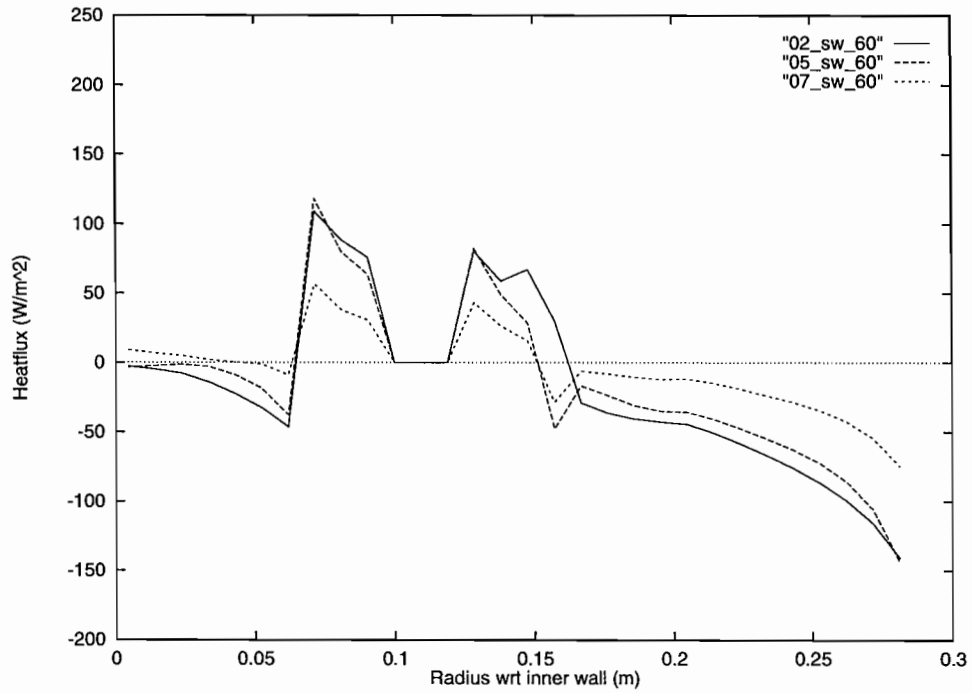

Figure 15: Heat flux on forward facing sidewall along radial direction 180 degrees, vertical upwards.

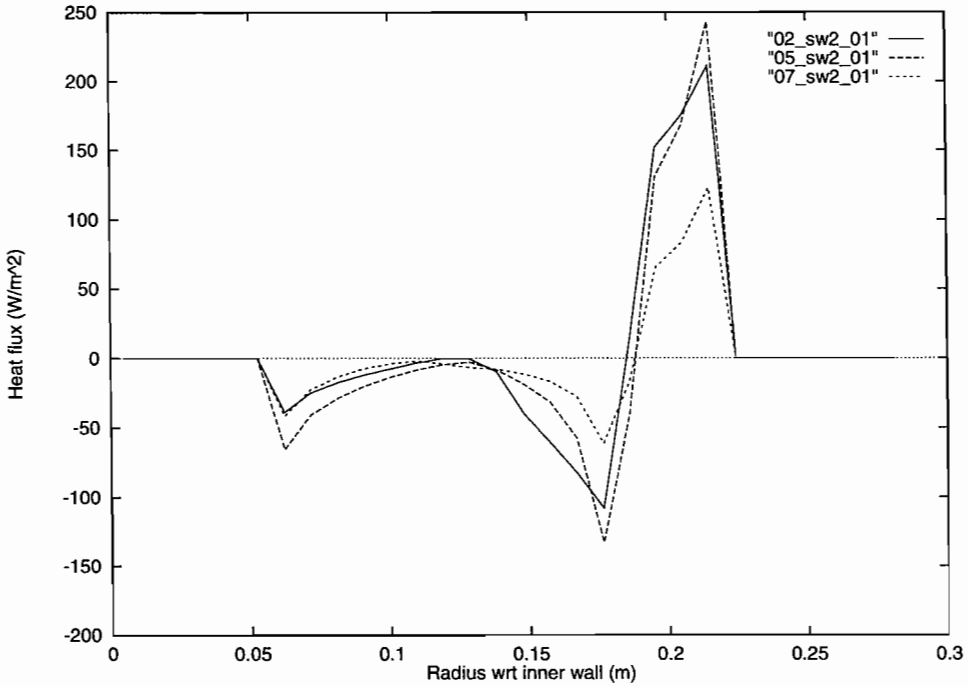

Figure 16: Heat flux on backward facing sidewall along radial direction 0 degrees, vertical downwards.

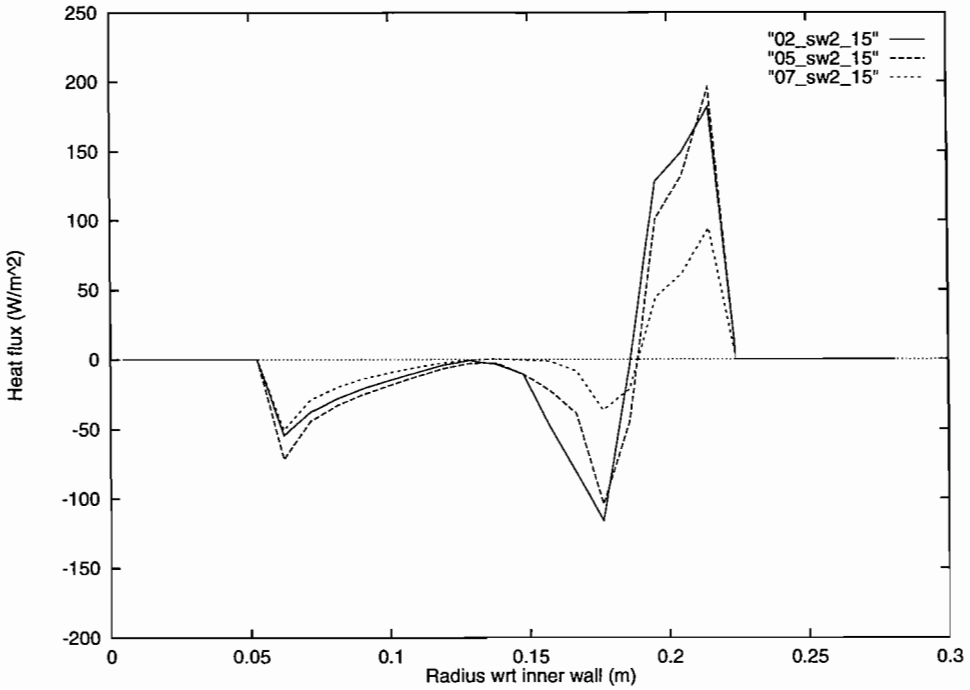

Figure 17: Heat flux on backward facing sidewall along radial direction 45 degrees.

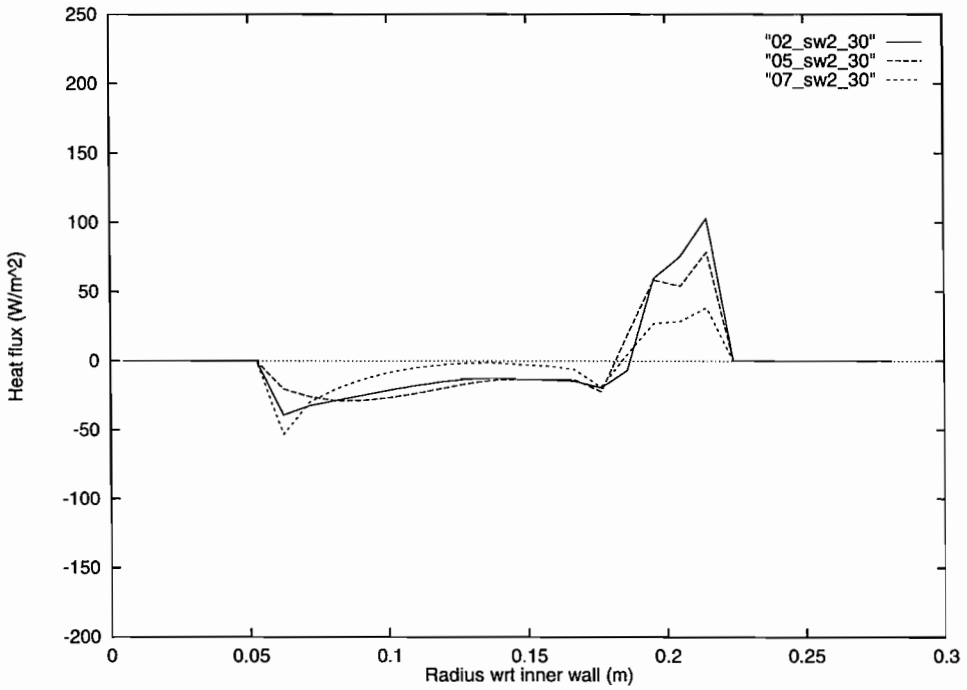

Figure 18: Heat flux on backward facing sidewall along radial direction 90 degrees, horizontal.

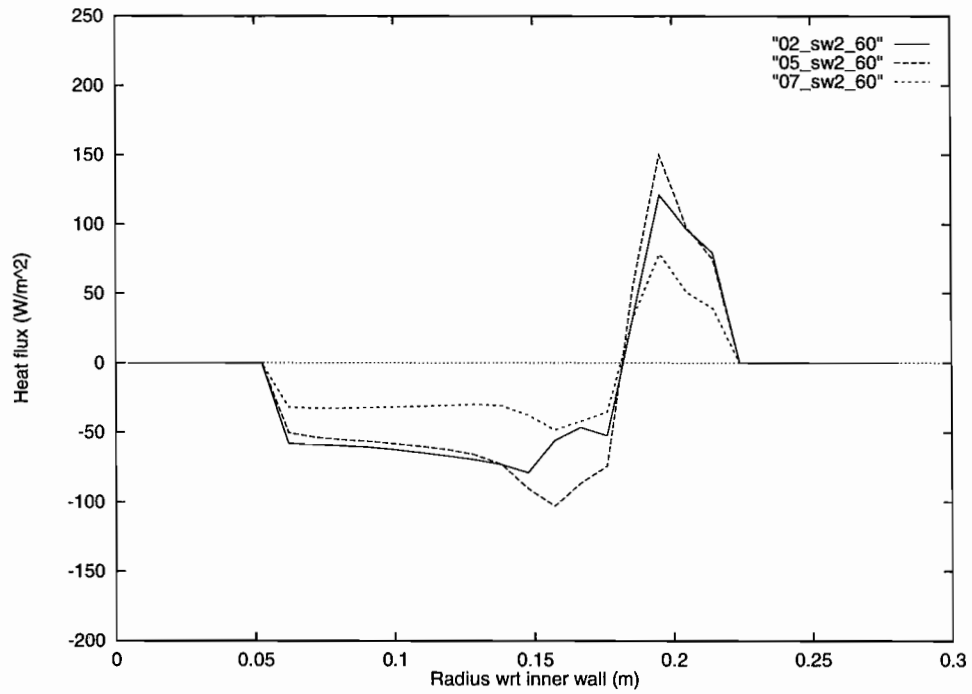

Figure 19: Heat flux on backward facing sidewall along radial direction 180 degrees, vertical upwards.

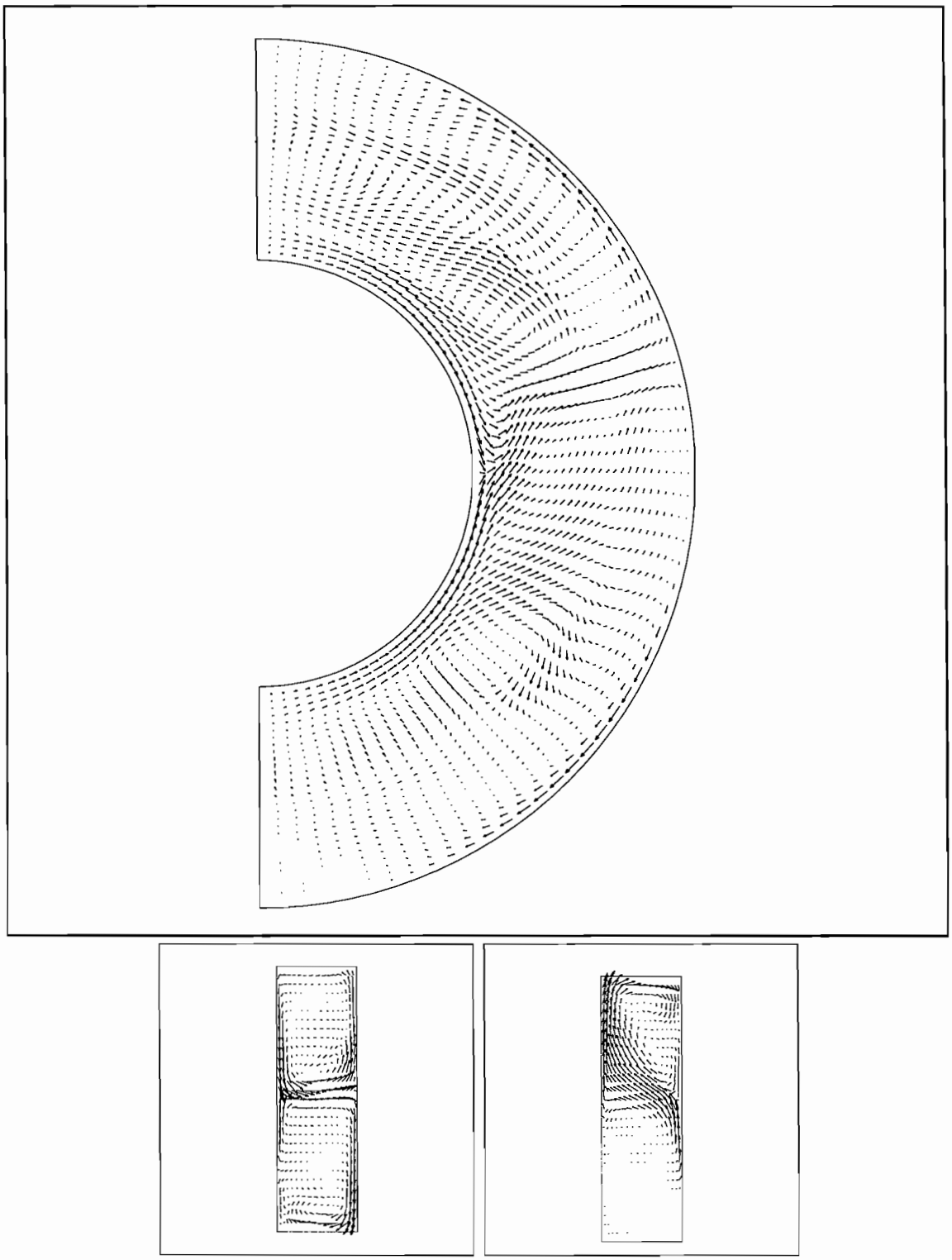

Figure 20: Velocity flow vectors for run m02. Results are shown for the centre plane, $y = 0.043m$ (top), and on the upper part of the $x = 0$ plane (bottom left) and the lower part of this plane (bottom right). The bottom left pattern shows a double circulation similar to that seen in the 2D results.

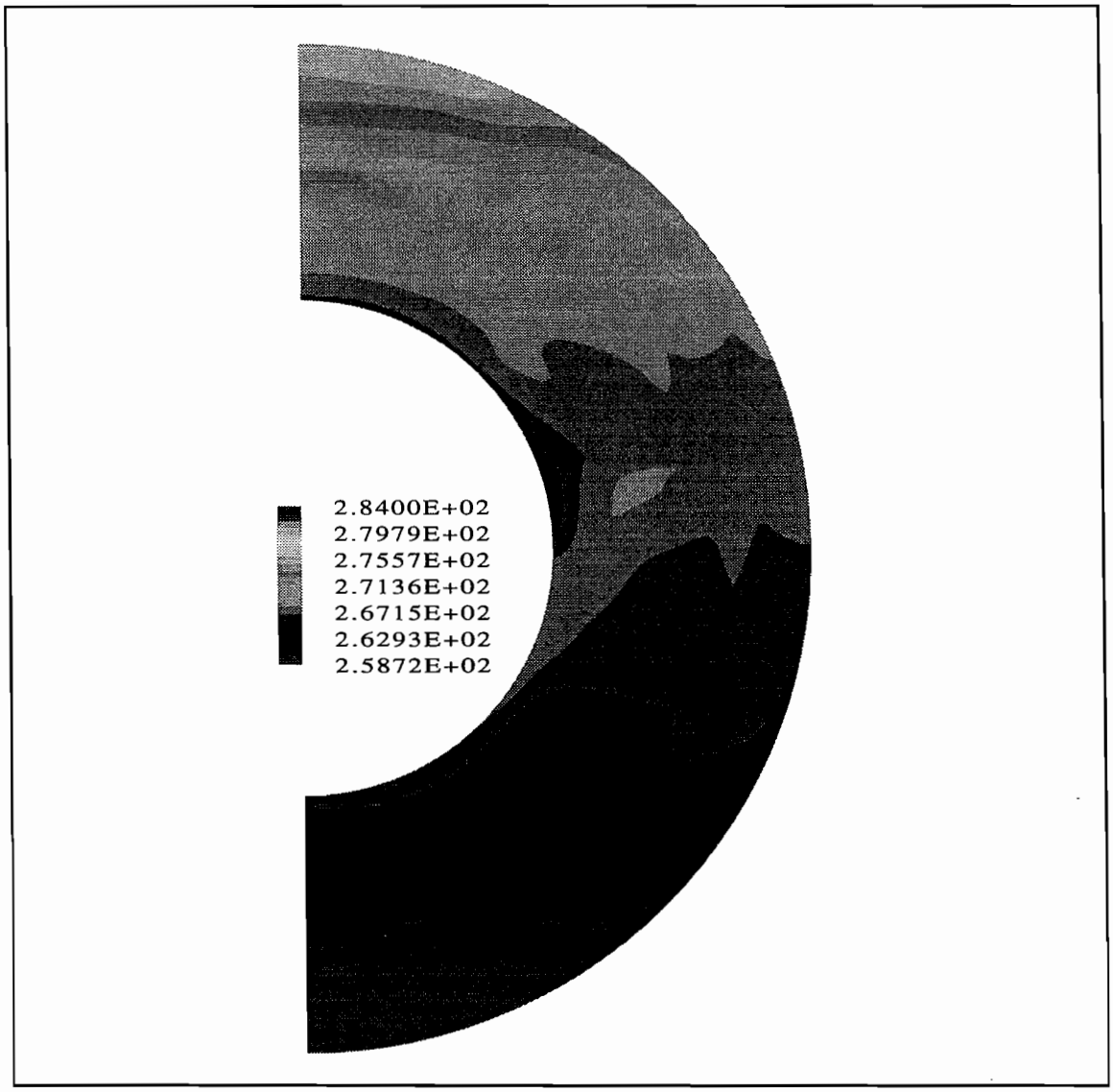

Figure 21: Final temperature distribution on the centre plane half way between the sidewalls for run m02.

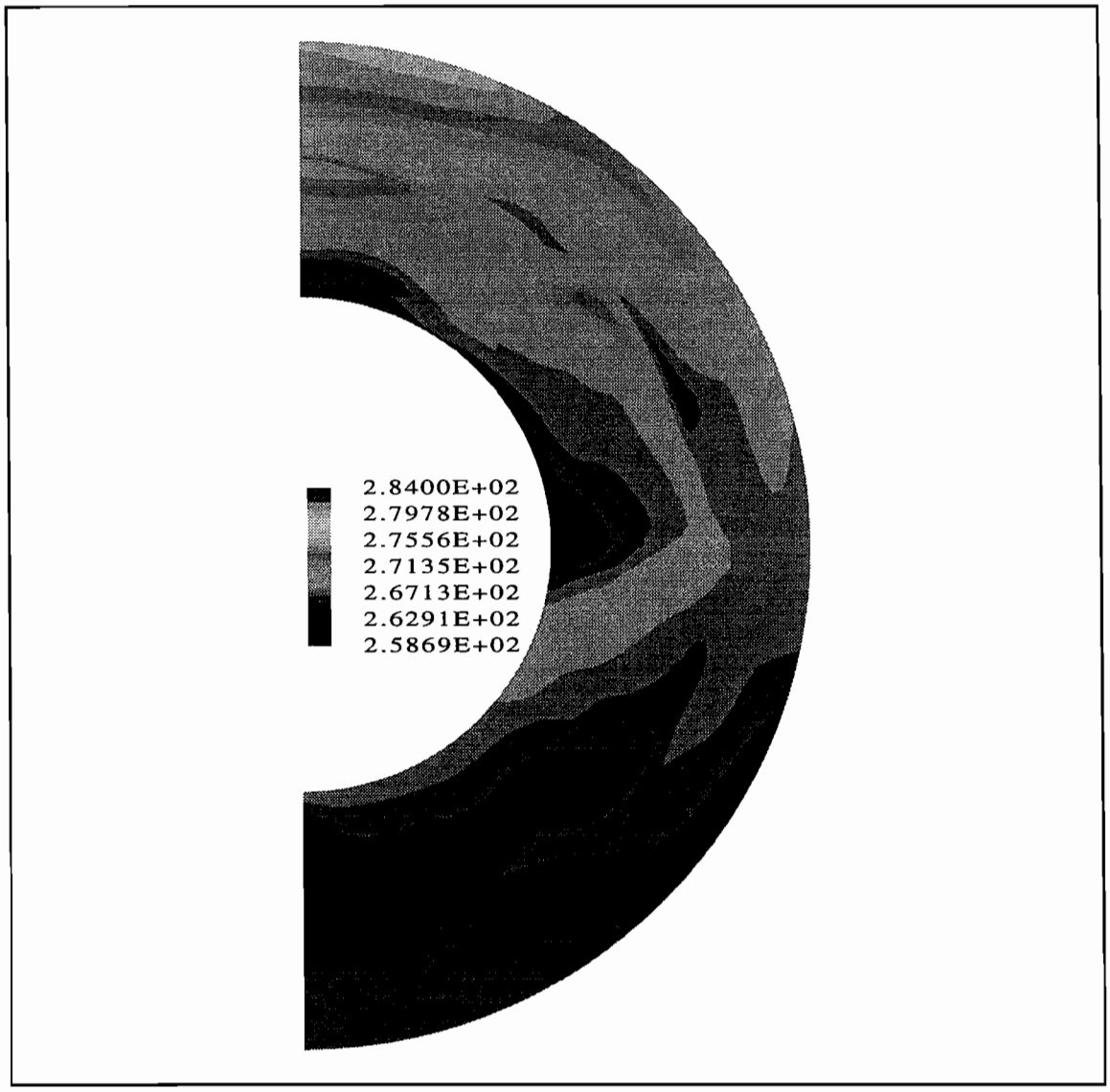

Figure 22: Final temperature distribution on the centre plane half way between the sidewalls for run m05.

Figure 23: Final temperature distribution on the centre plane half way between the sidewalls for run m07.

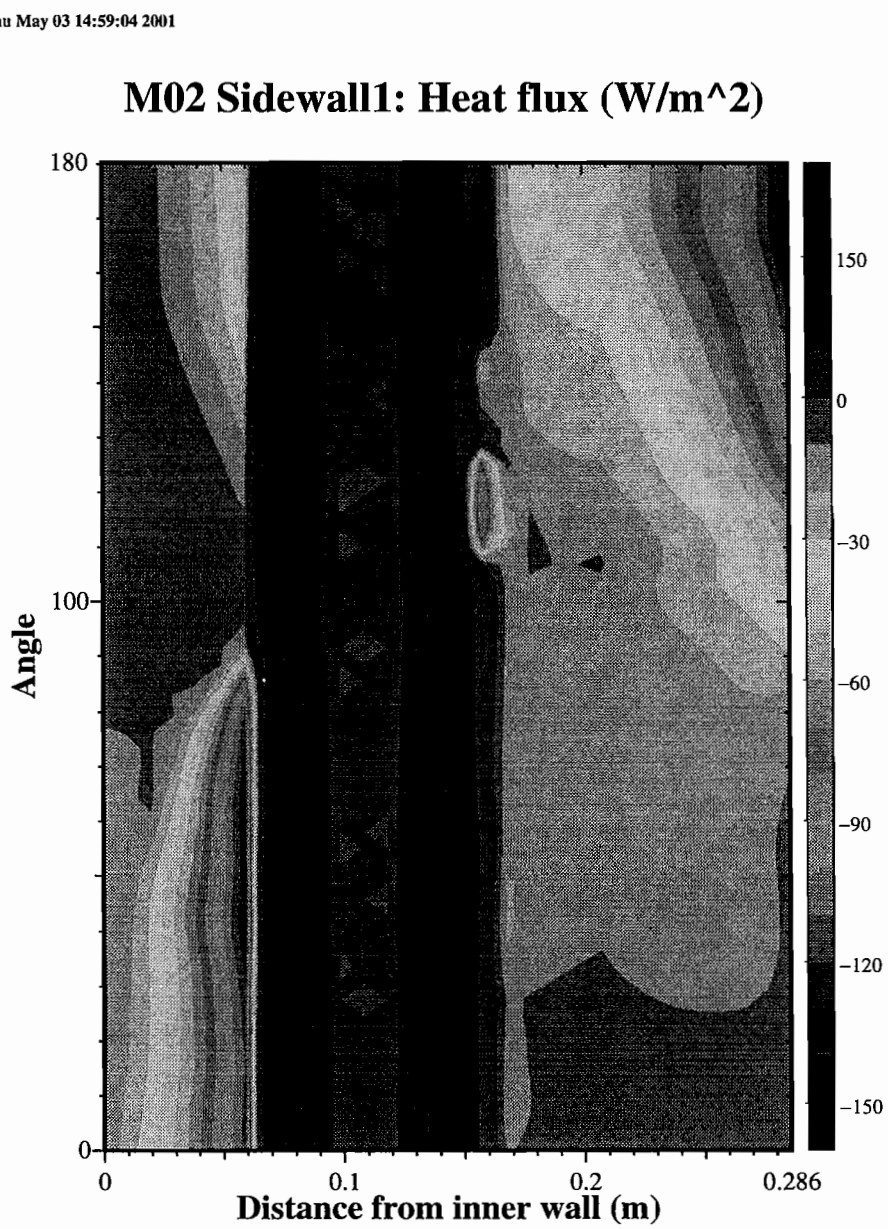

Figure 24: Contour plot of heat flux on forward facing sidewall, m02.

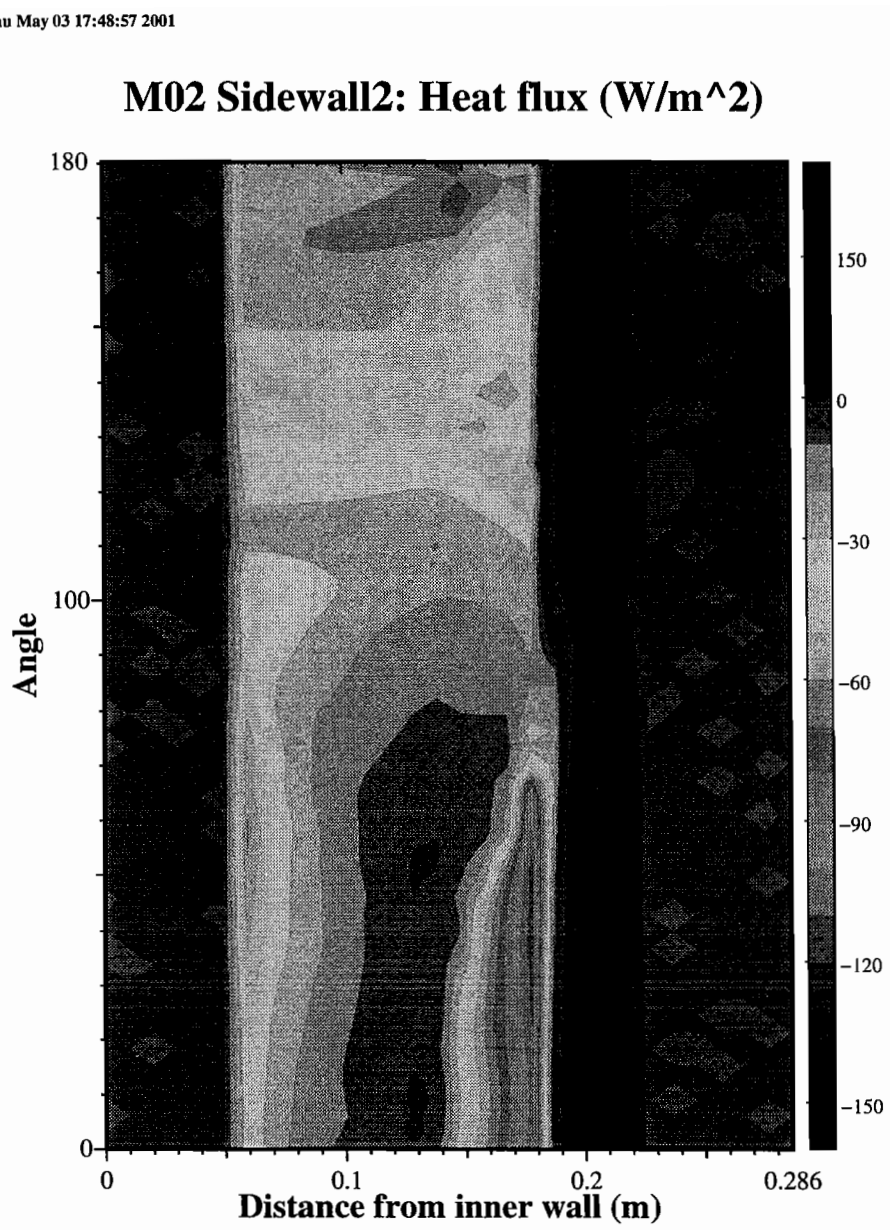

Figure 25: Contour plot of heat flux on back facing sidewall, m02.

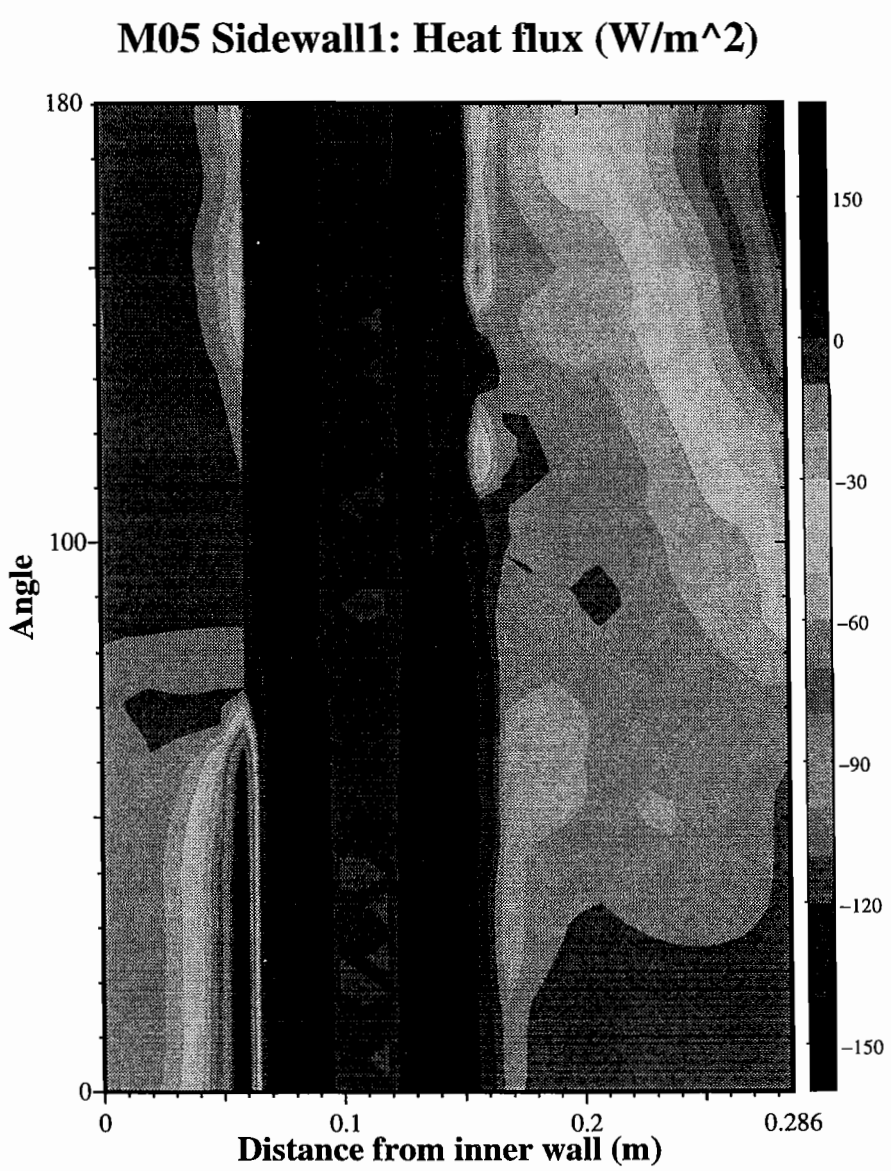

Figure 26: Contour plot of heat flux on forward facing sidewall, m05.

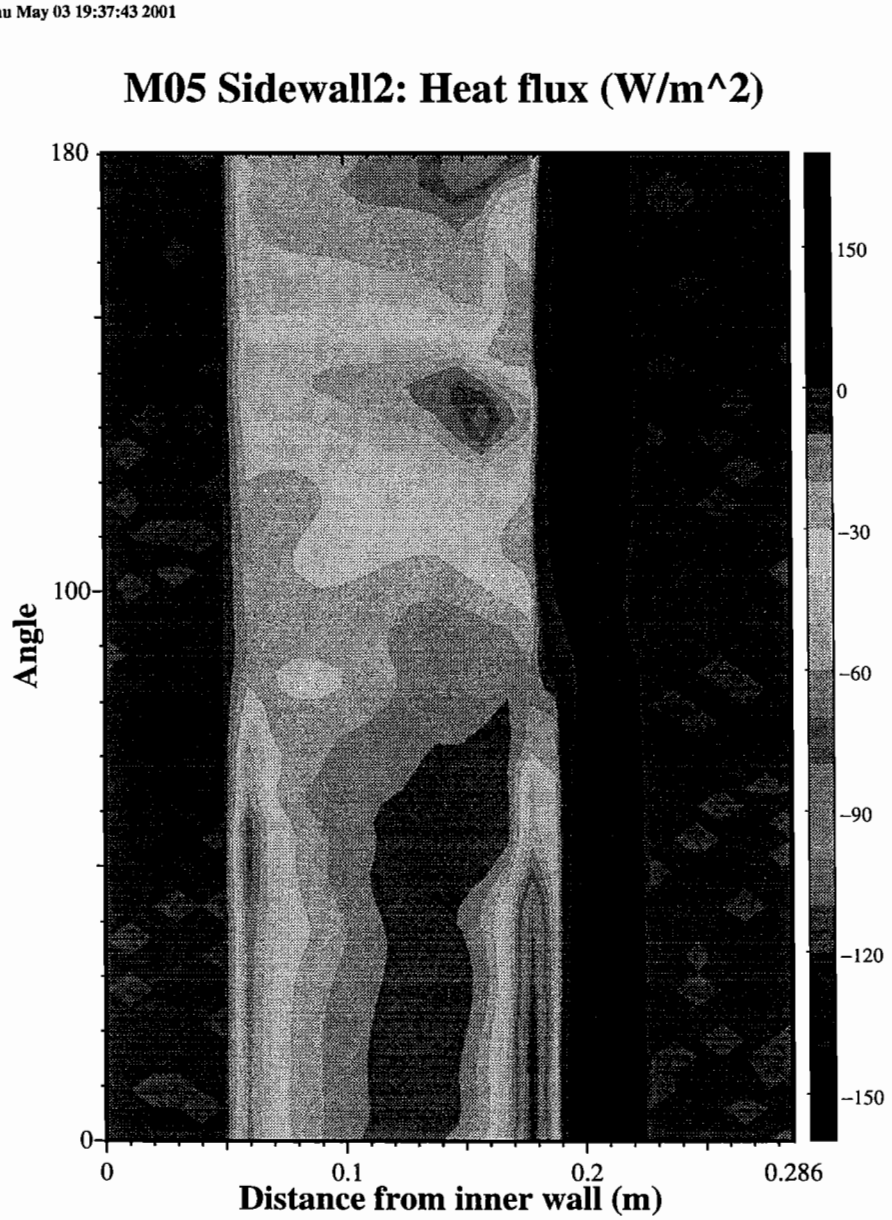

Figure 27: Contour plot of heat flux on back facing sidewall, m05.

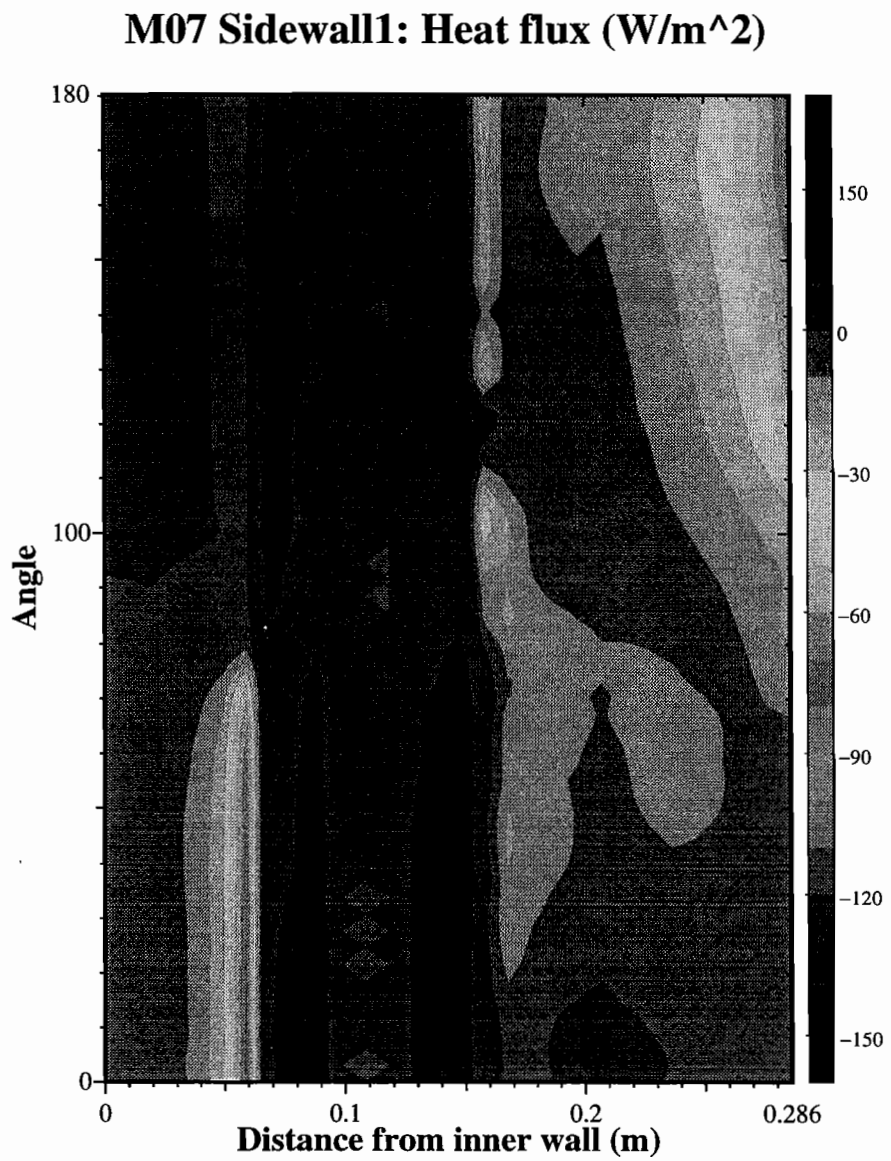

Figure 28: Contour plot of heat flux on forward facing sidewall, m07.

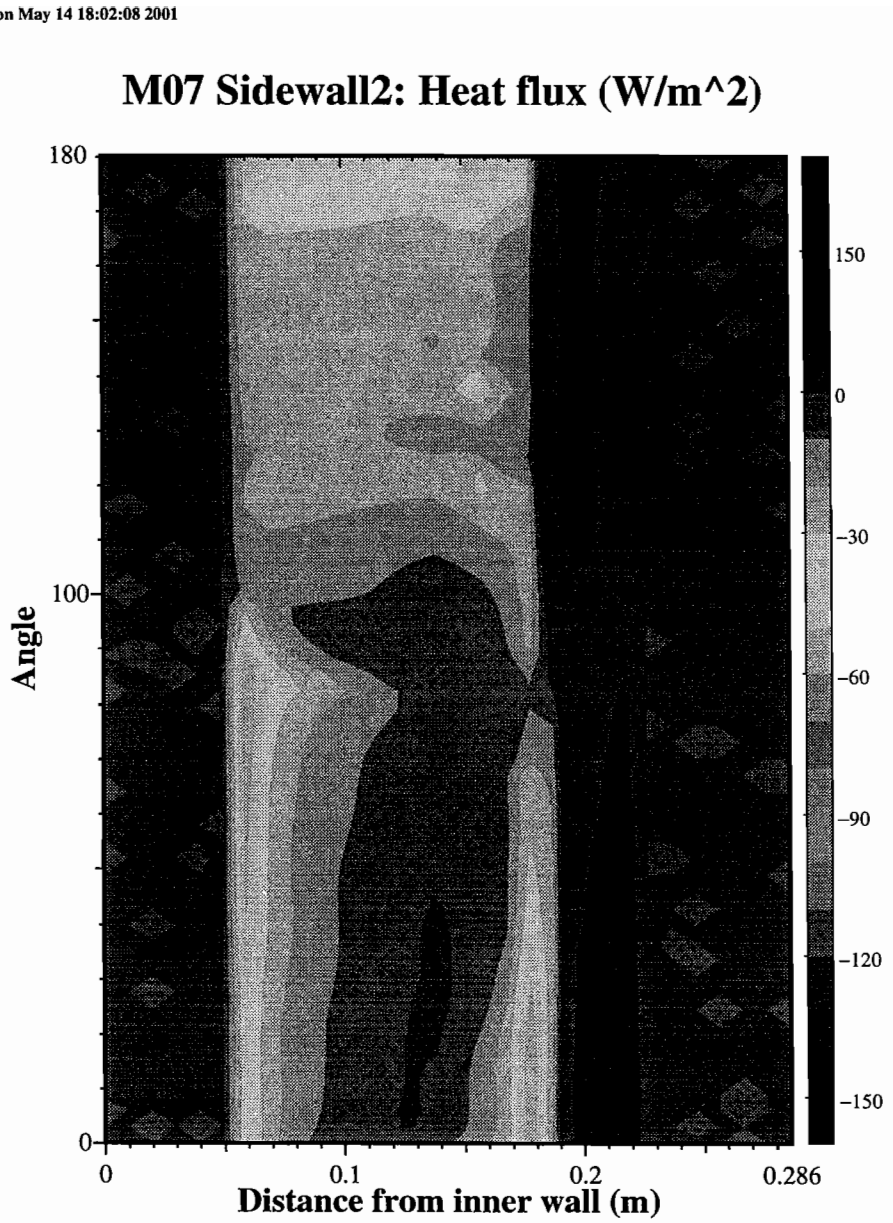

Figure 29: Contour plot of heat flux on back facing sidewall, m07.

5 Summary

The simulation results presented here are based on a model of the real system that contains a number of significant approximations in both the geometry of the enclosure and the heat transfer boundary conditions. Hence the predictions of the heat flux due to convection must be treated with some caution. To get results that are significantly more accurate would require detailed modelling of the complex geometry of the detectors themselves which would be a very time consuming task.

Comparison of the computational results with recent measurements on a mock up has shown broad agreement between the observed and predicted heat fluxes.

References

[1] "CFX 4.2: User manuals", CFX International, Harwell, Didcot, UK (1997).

[2] "Fundamentals of Fluid Mechanics", J.A.Schetz and A.E.Fuhs (Eds), John Wiley Inc., New York (1999).